

1 Microbial response to deliquescence of nitrate-rich soils in the 2 hyperarid Atacama Desert

3 Felix L. Arens^{1*}, Alessandro Airo^{1,2}, Christof Sager^{1,2}, Hans-Peter Grossart^{3,4}, Kai
4 Mangelsdorf⁵, Rainer U. Meckenstock⁶, Mark Pannekens⁶, Philippe Schmitt-
5 Kopplin^{7,8}, Jenny Uhl⁷, Bernardita Valenzuela⁹, Pedro Zamorano¹⁰, Luca
6 Zoccarato^{3,11,12}, Dirk Schulze-Makuch^{1,3,13}

7 ¹Technische Universität Berlin, Zentrum für Astronomie und Astrophysik, 10623 Berlin, Germany

8 ²Museum für Naturkunde, Leibniz-Institut für Evolutions- und Biodiversitätsforschung, 10115 Berlin, Germany

9 ³Department of Experimental Limnology, Leibniz-Institute of Freshwater Ecology and Inland Fisheries, 16775
10 Stechlin, Germany

11 ⁴Institute for Biochemistry and Biology, Potsdam University, 14469 Potsdam, Germany

12 ⁵Section Organic Geochemistry, Helmholtz Centre Potsdam GFZ German Research Centre for Geosciences,
13 Potsdam, Germany

14 ⁶Environmental Microbiology and Biotechnology, University of Duisburg-Essen, 45141 Essen

15 ⁷Helmholtz Zentrum München, Research Unit Analytical Biogeochemistry, 85764 Neuherberg, Germany

16 ⁸Technische Universität München, Chair of Analytical Food Chemistry, 85354 Freising, Germany

17 ⁹Laboratorio de Microorganismos Extremófilos, Instituto Antofagasta, Universidad de Antofagasta, Antofagasta
18 1240000, Chile

19 ¹⁰Departamento Biomédico, Facultad de Ciencias de la Salud, Universidad de Antofagasta; Antofagasta 1240000,
20 Chile

21 ¹¹Core Facility Bioinformatics, University of Natural Resources and Life Sciences (BOKU), 1190 Vienna, Austria

22 ¹²Institute of Computational Biology, University of Natural Resources and Life Sciences, 1180 Vienna, Austria

23 ¹³GFZ German Research Centre for Geosciences, Section Geomicrobiology, 14473 Potsdam, Germany

24

25 * Correspondence to: Felix L. Arens (f.aren@tu-berlin.de)

26

27 ABSTRACT

28 Life in hyperarid regions has adapted to extreme water scarcity through mechanisms like salt
29 deliquescence. While halite (NaCl) crusts have been intensively studied and identified as one
30 of the last habitats under hyperarid conditions, other less common hygroscopic salt crusts
31 remain unexplored. Here, we investigated newly discovered deliquescent soil surfaces in the
32 Atacama Desert, containing substantial amounts of nitrates, to evaluate their habitability for
33 microorganisms. We characterized the environment regarding water availability and
34 biogeochemistry. Microbial abundances and composition were determined by cell cultivation
35 experiments, 16S rRNA gene sequencing, and membrane phospholipid fatty acid (PLFA)
36 analysis while microbial activity was assessed by analyzing ATP and the molecular
37 composition of organic matter. Our findings reveal that while the studied hygroscopic salts
38 provide temporary water, microbial abundances and activities are lower than in non-
39 deliquescent soil surfaces. Intriguingly, the deliquescent crusts are enriched in geochemically
40 degraded organic matter, indicated by the molecular composition. We conclude that high nitrate
41 concentrations in the hyperarid soils suppress microbial activity but preserve eolian-derived
42 biomolecules. These insights are important for assessing the habitability and searching for life
43 in hyperarid environments on Earth and beyond.

Deleted: by using

Deleted: and

Deleted: , PLFA, and

47 1 INTRODUCTION

48 The Atacama Desert is one of the driest and oldest deserts on Earth with hyperarid conditions established in the
49 Oligocene (Dunai et al., 2005; Jordan et al., 2014). Over the last two decades, the Atacama Desert has been
50 intensively studied as a Mars analog and for the dry limits of life along aridity gradients progressing towards
51 hyperaridity (Quade et al., 2007; Schulze-Makuch et al., 2018). Vegetation density decreases with increasing
52 aridity until vascular plants become absent in the hyperarid core (Quade et al., 2007). It has long remained unclear
53 whether there is active life or whether recovered DNA is only blown in from the atmosphere and slowly decaying
54 (Navarro-Gonzalez et al., 2003; Lester et al., 2007). However, later studies showed that microbial life can indeed
55 survive and temporally thrive after rare rain events within the hyperarid core of the Atacama Desert (Warren-
56 Rhodes et al., 2006; Wierzchos et al., 2006; Connon et al., 2007; Wierzchos et al., 2012; Schulze-Makuch et al.,
57 2018; Hwang et al., 2021; Schulze-Makuch et al., 2021).

58 With increasing aridity, life retreats from the surface into the subsurface. Photosynthesis-based microbial
59 communities inhabit hypolithic and endolithic habitats under translucent rocks and crusts or within their pore space
60 (Warren-Rhodes et al., 2006; Wierzchos et al., 2011). These micro-environments provide shelter against UV-
61 radiation while receiving sunlight and buffering evaporation and temperature fluctuation. These ecosystems can
62 be found widely in the arid part of the Atacama Desert and even sporadically in the hyperarid region (Warren-
63 Rhodes et al., 2006). In contrast to rain and fog, deliquescence is thought be the last source of liquid water, enabling
64 microbial colonization in a unique ecological sequence towards increasing aridity (Davila and Schulze-Makuch,
65 2016). The last islands of habitability towards the dry limit of life are found inside surficial salt crusts (Wierzchos
66 et al., 2006; Davila and Schulze-Makuch, 2016; Schulze-Makuch et al., 2021). These can provide liquid water
67 through deliquescence of hygroscopic salts, i.e., halite (NaCl), absorbing water vapor from humid air (>75 %
68 relative humidity (RH) for NaCl at 20 °C) and forming a saturated brine on the salt crust surface and within the
69 soil pore space (Davila et al., 2013; Robinson et al., 2015; Maus et al., 2020).

70 In the Atacama Desert, salt crusts are commonly found in dried-out saline lakes, locally called salars, with
71 prominent salt aggregates at the surface, composed of halite with varying fractions of gypsum and lithic detrital
72 clast (Stoertz and Ericksen, 1974; Wierzchos et al., 2006; Robinson et al., 2015; Schulze-Makuch et al., 2021).
73 The so-called salt nodules are formed by cycles of deliquescence and efflorescence and are superimposed by eolian
74 erosion (Artieda et al., 2015). The Atacama Desert experiences pronounced diurnal climate shifts, where nighttime
75 air humidity approaches 100% RH as temperatures drop, facilitating regular deliquescence. As temperatures rise
76 with sunrise, RH can fall below 5%, triggering efflorescence (McKay et al., 2003). Apart from salars, salt
77 accumulations are generally found within the Atacama Desert in the subsurface of alluvial deposits, which have
78 accumulated over millions of years (Ericksen, 1981; Ewing et al., 2006). The prolonged hyperarid conditions
79 resulted in atmospheric salt accumulation and a post-depositional separation within the soil column through rare
80 rain water infiltration (Ewing et al., 2006; 2008; Arens et al., 2021). As a result, highly soluble NaCl and NaNO₃

81 migrate deeper into subsurface horizons, locally called caliche. The soil above is dominated by sulfate. Close to
82 the surface, the soil is exceptionally porous (chusca) and becomes more firmly cemented in the subsurface (costra)
83 (Ericksen, 1981). Thermal stress and salt dehydration lead to cracks which can develop into sand wedges that
84 shape the typical hexagonal and orthogonal soil polygons in the Atacama Desert (Ewing et al., 2006; Pfeiffer et
85 al., 2021; Sager et al., 2021) (Fig. 1).

Deleted: absolute desert

Deleted: one of the

Deleted: In contrast to rain and fog, deliquescence might be the last source of liquid water, enabling microbial colonization in a unique ecological sequence towards increasing aridity (Davila and Schulze-Makuch, 2016).

Formatted: Font: Italic

Deleted: They are mainly composed of halite with varying fractions of gypsum and lithic detrital clasts (Wierzchos et al., 2006; Robinson et al., 2015; Schulze-Makuch et al., 2021).

Deleted: and hygroscopic

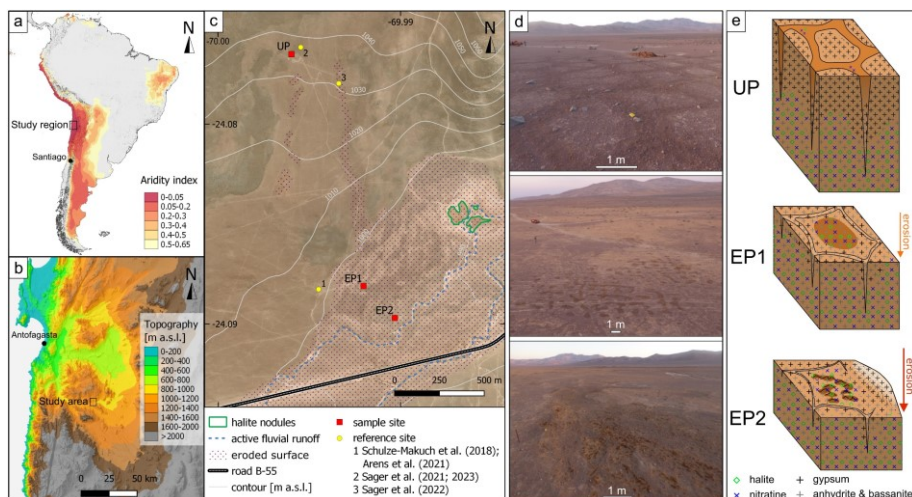


Figure 1: Overview of the study area. a) Map of South America with color code for the aridity index with <math><0.05</math> being hyperarid (Zomer et al., 2022). b) Topographic map of the study region, with the Yungay valley, 60 km southeast of Antofagasta, where the study area is located. c) Landsat-8 satellite image of the study area with 10 m interval isohyets, showing the three sample sites and relevant reference sites. The purple dotted area marks surface erosion and the blue dashed line indicates main run-off channels, active during the last major rain events (2017). The nearest observed salt nodules are outlined in green. d) Aerial photos of the study sites during morning hours. e) Sketches of the soil structures at each site with salt distribution. Darker surface areas indicate potential deliquescence.

Further, local eolian erosion can lead to the exposure of salt-rich subsurfaces down to the *caliche* horizon (Sager et al., 2022). Similar to halite nodules, salt-encrusted surfaces can form here, composed of sulfate, chloride, and nitrate salts, that develop similar efflorescent morphologies (Fig. 2). While halite-rich soil crusts have been shown to be inhabited by microbes (Wierzchos et al., 2006), the potential role of nitrate-rich soil crusts as microbial habitats remains unclear. This study aims to characterize hygroscopic nitrate-rich soil crusts within the hyperarid Atacama Desert, employing an interdisciplinary approach that integrates geochemical, biogeochemical, and microbiological methods. The goal is to unravel the significance of nitrates for microbial life in one of the most arid regions on Earth, serving as an outstanding Martian analog. These hypersaline environments are especially interesting for the search for life on Mars where nitrates have been detected (Stern et al., 2015), as these may provide a last refuge for putative Martian organisms, potentially providing water (Davila and Schulze-Makuch, 2016) and could serve as excellent candidates for the preservation of biosignatures in the shallow subsurface being protected by irradiation but still accessible for future sampling missions (Fernández-Remolar et al., 2013).

Deleted: Analogous

2 METHODS

2.1 Study area and sampling

The here investigated soil surfaces are located in the Yungay valley within the hyperarid Atacama Desert, Chile (Fig. 1a, b) (UP: 24.076S 69.995W; EP1: 24.088S 69.992W; EP2: 24.090S 69.991W). The sample sites are located on a distal part of an alluvial fan, which developed polygonal patterned grounds on its surface (Fig. 1c). Deliquescence-induced water uptake capacities and potential changes in microbial activity were evaluated by taking samples in the morning (potentially moist) and in the evening (dry). At each sampling site, surface samples in 0–5 cm depth were taken in the deliquescence affected area and in adjacent areas which were not affected by deliquescence. Roughly 100 g sample material for geochemical analysis were collected in PE bags. Triplicate samples for water activity and content were stored in 100 mL glass bottles with PTFE sealed lids at 4 °C until analysis. Biological samples were sampled in triplicates in 50 mL centrifuge tubes and stored at –20 °C until analysis. Precautions were taken to keep all samples sterile and to avoid cross-contamination by wearing nitrile gloves as well as by wiping and flaming the sampling tools using ethanol before each use. Sampling took place between 11.3. and 14.3.2019.

131 **2.2 Environmental monitoring**

132 Temperature and RH of the air (1 m above ground) in the study area was recorded between 2018 and 2019 using
133 environmental loggers U23-001 by Onset (USA). Soil electrical conductivity was measured on selected surfaces
134 in 0-5 cm depths using a CR10 (Campbell Scientific, USA). Aerial images were taken by a DJI Phantom 4
135 unmanned aerial vehicle and later processed into orthophotos and DEMs with Agisoft Metashape Pro software.
136 Field images were calibrated with SpyderCHECKR®24 (datacolor, Switzerland) and post-processed for color
137 correction with checkr24 (datacolor, Switzerland) software.

138 **2.3 Water activity and content analysis**

139 Triplicate samples were analyzed for water activity and content analysis. The water content of the collected
140 samples was determined by the weight loss after drying at 60 °C for 24 h to avoid the dehydration of gypsum. The
141 water activity was analyzed with a LabMaster-aw neo (Switzerland) equipped with an electrolytic sensor.

142 **2.4 Geochemical and mineral analyses**

143 *2.4.1 Mineral analysis*

144 The bulk mineralogy was analyzed via powder XRD. 5 g sample aliquots were dried at 60 °C and ground to
145 powder. XRD analysis was performed by using a D2 Phaser (Bruker, USA) powder diffractometer. The X-ray
146 source is a Cu K α radiation (K-alpha1= 1.540598 Å, K-alpha2=1.54439 Å) with a performance of 30 kV and
147 10 mA. A step interval of 0.013° 2 θ with a step-counting time of 20 s was used in a scanning range from 5° to
148 90° 2 θ . Evaluation was conducted semi-quantitatively using the “Powder Diffraction File Minerals 2019”
149 (International Centre of Diffraction Data) together with the software High Score from PANalytical (Netherlands).

150 *2.4.2 Ion chromatography*

151 Anionic species (Cl⁻, NO₃⁻, SO₄²⁻) were measured by ion chromatography (DIONEX DX-120 ion chromatograph,
152 Thermo Fisher Scientific Inc., USA). Samples were dried at 60 °C, sieved dry to <2 mm grain size, and leached in
153 duplicates with a 1:10 ratio (sample:water (w/w)). Samples were measured in duplicates and blanks were measured
154 alongside the samples for quality control.

155 *2.4.3 Elemental analysis*

156 Total carbon, nitrogen, and sulfur were measured on homogenized, powdered samples with a Vario Max CNS
157 (Elementar GmbH, Germany) at 1140 °C combustion temperature. TOC was measured on a Vario Max C by
158 combustion at 600 °C. Measurements were performed in duplicates with 1 g of sample ~~alongside glutamic acid~~
159 standards for organic carbon and blanks were used to determine detection limits of 0.01 wt% for C, N, S and
160 0.03 wt% for TOC. TIC was calculated as the difference between total carbon and organic carbon.

Deleted: and

161 **2.5 Biological analyses**

162 *2.5.1 Adenosine triphosphate (ATP) analysis*

163 Sediment samples were placed in a sterile autoclave bag and crushed into smaller pieces (up to a maximum
164 diameter of approximately 1 cm) using a hammer. 6 g of sediment or crushed rock samples were introduced into
165 a 50 mL centrifuge tube, and 5 mL of ice-cold sodium phosphate buffer (0.12 M Na₂HPO₄, NaH₂PO₄, pH = 8.0)
166 was added. Samples were shaken on an orbital shaker for 5 min at 150 rpm, cooled on ice for 3 min, and shaken
167 again for another 5 min. Samples were then centrifuged at 4 °C and 500 g for 10 min. The supernatants, which
168 contain the tATP, were recovered in a 15 mL centrifuge tube, and 1 mL of sodium phosphate buffer was added to
169 the sediment samples. The procedure was repeated 3 times and supernatants were collected. This was done
170 separately for the tATP and iATP. For the iATP, the collected suspensions were centrifuged at 4 °C and 4,600 g
171 for 60 min. Cell pellets containing iATP were re-suspended in 4 mL of sodium phosphate buffer and the particles
172 in the solution were allowed to settle for approximately 30 min before samples were subjected to ATP analysis. All
173 samples were processed in triplicates. ATP was quantified using the luciferase-based BacTiter-Glo™ Microbial
174 Cell Viability Assay (Promega, USA). Measurements for the iATP were carried out according to the

176 manufacturer's protocol, using a 6-point calibration curve with ATP concentrations ranging from 10 pM to 1 μM
177 in a 0.12 M sodium phosphate buffer. For the tATP a 5-step standard addition with 1, 2, 3, 4 μL of 0.1 μM ATP
178 was applied to avoid matrix effects potentially caused by the dissolved soil salts (supplementary information S6).
179 Finally, 100 μL of sample solution, blank, or standard were mixed with 100 μL of BacTiter-Glo™ reagent, which
180 was prepared on the day before measurement and kept at room temperature until measurements were performed.
181 5 minutes after mixing, luminescence was recorded using a Glomax 20/20 luminometer (Promega, USA).

182 2.5.2 Phospholipid fatty acid (PLFA)

183 PLFA extraction and subsequent analysis were conducted with the procedure described in detail by [Zink and](#)
184 [Mangelsdorf](#) (2004) and [Sager et al.](#) (2023). PLFAs were obtained from intact membrane phospholipids by
185 applying an ester cleavage procedure (Müller et al., 1990). Hereby, the phospholipid linked fatty esters are directly
186 transformed into their respective fatty acid methyl esters (PLFAs) using trimethylsulfonium hydroxide.
187 Subsequently, the PLFAs were measured on a trace gas chromatograph (GC) 1310 (Thermo Scientific, USA)
188 coupled to a TSQ 9000 mass spectrometer (MS) (Thermo Scientific, USA). The GC was equipped with a cold
189 injection system operating in the splitless mode and a SGE BPX 5 fused-silica capillary column (50 m length,
190 0.22 mm ID, 0.25 μm film thickness) with initial temperature of 50 °C (1 min isothermal), heating rate 3 °C min⁻¹
191 to 310 °C, held isothermally for 30 min. Helium was used as carrier gas with a constant flow of 1 mL min⁻¹. The
192 injector temperature was programmed from 50 to 300 °C at a rate of 10 °C s⁻¹. The MS operated in electron impact
193 mode at 70 eV. Full-scan mass spectra were recorded from m/z 50 to 650 at a scan rate of 1.5 scans s⁻¹. [PLFAs](#)
194 [were identified according to their chromatographic behavior compared to a mixed fatty acid standard \(containing](#)
195 [the usual saturated, unsaturated and branched fatty acids\) and/or their characteristic mass spectra. To quantify the](#)
196 [PLFAs, we added a deuterated phospholipid standard \(PC₃₄, phosphatidyl choline with two deuterated](#)
197 [tetradecanoic ester side chains\) as internal standard after the lipid extraction.](#) A blank was prepared and measured
198 alongside the samples for quality control.

199 2.5.3 16S rRNA gene sequencing

200 DNA extraction of soil samples was performed based on a slightly modified protocol of Nercessian et al.,
201 (Nercessian et al., 2005) with sample aliquots of 5 g. In brief, cell lysis was performed using glass beads (100–500
202 μm) in the presence of lysozyme, proteinase K and cetyltrimethyl ammonium bromide (CTAB). DNA purification
203 was facilitated by the addition of Phenol-Chloroform and polyethylene glycol (PEG) (Neubauer et al., 2021). The
204 V3-V4 region of the 16S rRNA was amplified using the S-D-Bact-0341-b-S-17 / S-D-Bact-0785-a-A-21 primer
205 pair (Mitra et al., 2013), while library preparation and sequencing were carried out on an Illumina MiSeq
206 instrument (Illumina, USA).

207 Demultiplexing, removal of primer and adapter sequences were performed using Cutadapt v3.7 (Martin, 2011).
208 Fastq files are deposited in the SRA. Additional quality filtering and trimming, identification of unique amplicon
209 sequence variants (ASVs) and paired reads merging were performed using the DADA2 v1.20 (Callahan et al.,
210 2016) following the standard pipeline with default values (we set pool = T for the dada() function and
211 method = "consensus" for the removeBimeraDenovo() function). Taxonomy was assigned to ASVs using SINA
212 v1.7.2 (Pruesse et al., 2012) against the SILVA reference database (SSU NR 99 v138.1; (Quast et al., 2012)).

213 ASVs having less than five total reads or which occurred in less than three samples were removed from
214 downstream analyses. Alpha and beta diversity analyses were performed in R phyloseq package (McMurdie and
215 Holmes, 2013). Alpha diversity (Chao1) was calculated and the function *estimateR* (R package vegan) was used
216 to estimate ASV richness as it accounts for differences in library sizes. For the Principal Coordinate Analysis
217 (PCoA), ASV counts have been centered-log-ratio transformed using the function *decostand* (method = "rclr",
218 package vegan). The Aitchison distance was then obtained with the vegan function *vegdist* (method = "euclidean",
219 R package vegan) and the PCoA was plotted using *plot_ordination* (method = "PCoA", R package phyloseq,
220 (Wickham et al., 2016)). Distance-based linear modeling was performed using normalized environmental variables
221 (function *decostand*, method = "normalize"), and significant variables were visualized via canonical analysis of
222 principal coordinates (CAP) plot. The CAP was carried out to relate bacterial communities to different
223 environmental variables (including EC, gypsum, Cl⁻, NO₃⁻, ATP, TOC).

224 2.5.4 Cell cultivation experiments

225 Microbial cell abundance was estimated by carrying out cultivation experiments following the protocol by (Knief
226 et al., 2020). In triplicates, 5 g sample aliquot was suspended in 25 mL of sterile phosphate buffer solution

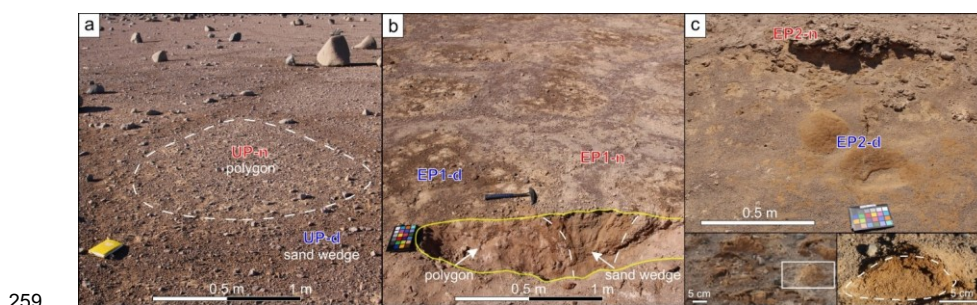
227 (120 mM, pH = 8) and incubated for 30 min at 60 rpm at room temperature in a shaker (LabNet, USA) followed
228 by 2 min ultrasonication in a water bath (Emlasonic S 30H, Germany). 100 μ L of the obtained suspensions were
229 spread in triplicates on agar plates. Nutrient broth medium was used for the growth of bacterial cells consisting of
230 3 g L⁻¹ yeast extract, 3 g L⁻¹ peptone, and 15 g L⁻¹ agar. Plates were incubated at room temperature and evaluated
231 for bacterial growth after 4 weeks by counting the colony forming units (CFUs). Bacterial genomic DNA of
232 individual CFUs was extracted using the Wizard Genomic DNA Purification Kit (Promega, Madison, WI, USA)
233 and amplified through PCR targeting the universal 16S rDNA region with bacterial primers 27F and 1525R
234 (Altschul et al., 1997). PCR reactions utilized the Go Taq Green Master Mix kit (Promega, Valencia, CA, USA),
235 with cycling conditions including an initial denaturation at 95 °C for 5 min, followed by 35 cycles of denaturation
236 (95 °C for 30 s), annealing 55 °C for 30 s, and extension 72 °C for 1.5. PCR products' integrity was confirmed
237 through gel electrophoresis, and the amplicons were sequenced at Macrogen (Republic of Korea) and analyzed for
238 comparison with GenBank (NCBI) sequences.

239 2.5.5 Profiling organic matter via FT-ICR-MS

240 The same extraction and analytical protocol as for similar studies in the region were used to gain comparability
241 (Schulze-Makuch et al., 2018; Schulze-Makuch et al., 2021). Mass spectra were acquired in negative electrospray
242 ionization (ESI) mode using a Solarix Qe FT-ICR-MS equipped with a 12 T superconducting magnet and coupled
243 to an Apollo II ESI-source (Bruker Daltonics, Germany). Methanolic soil extracts were continuously infused with
244 a flow rate of 120 μ L h⁻¹. Spectra accumulated 500 scans within a mass range of 147 to 1000 m/z. An internal
245 calibration was performed with a mass accuracy of <0.1 ppm, and peaks with a signal to noise ratio >6 were picked.
246 Formula assignment was performed with in-house written software (NetCalc) using a network approach to
247 calculate chemical compositions containing carbon, hydrogen, and oxygen, as well as nitrogen and/or sulfur. The
248 mass accuracy window for the formula assignment was set to ± 0.5 ppm, and the assigned formulas were validated
249 by setting sensible chemical constraints (N rule; O/C ratio ≥ 1 ; H/C ratio $\leq 2n + 2$ (maximum possible carbon
250 saturation, with n defined as CnHn+2 for any formula), double bond equivalents) in conjunction with isotope
251 pattern comparison. Results were visualized using van Krevelen diagrams in which the hydrogen to carbon ratio
252 (H/C) was plotted against the oxygen to carbon ratio (O/C). The different bubble sizes represent the intensity of
253 the characteristic molecular formula within the respective sample.

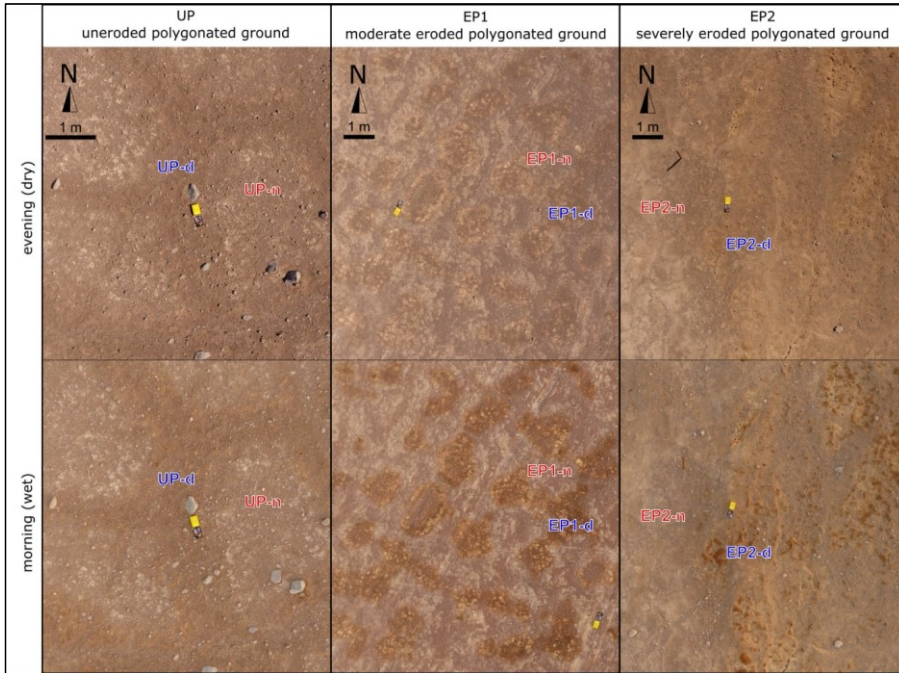
254 3 RESULTS

255 The influence of deliquescence on soil habitability was investigated on three selected sampling sites on polygonal
256 soils: uneroded (UP), moderately eroded (EP1) and strongly eroded (EP2), where repeated deliquescence was
257 observed in varying intensities (Fig. 1, 2). This was most pronounced at the EP2 site, which we chose as our
258 primary target.



259 Figure 2: Images of the sample sites. Bright soil colors indicate sulfates, dark soil colors indicate nitrates and chlorides. a) UP
260 site with the darker sand wedge surface, enclosing the brighter polygon surface. Example polygon outline with white dashes.
261 b) EP1 site with dark polygon surface, surrounded by bright sand wedges. Excavation pit outlined yellow, border between
262 polygon and sand wedge marked with white dashes. c) EP2 site with small troughs formed by eolian erosion exposing nitrate-
263 and chloride-rich soil which appear dark brown. Remains of the overlying *chusca* are visible in the background. Left inlet:
264 detailed image of efflorescent morphologies within EP2-d. White box indicates area of right inlet: cross section (white dashed
265 line) of an efflorescence dome. Moisture reached a few centimeters into the ground. The soil below remained dry.
266

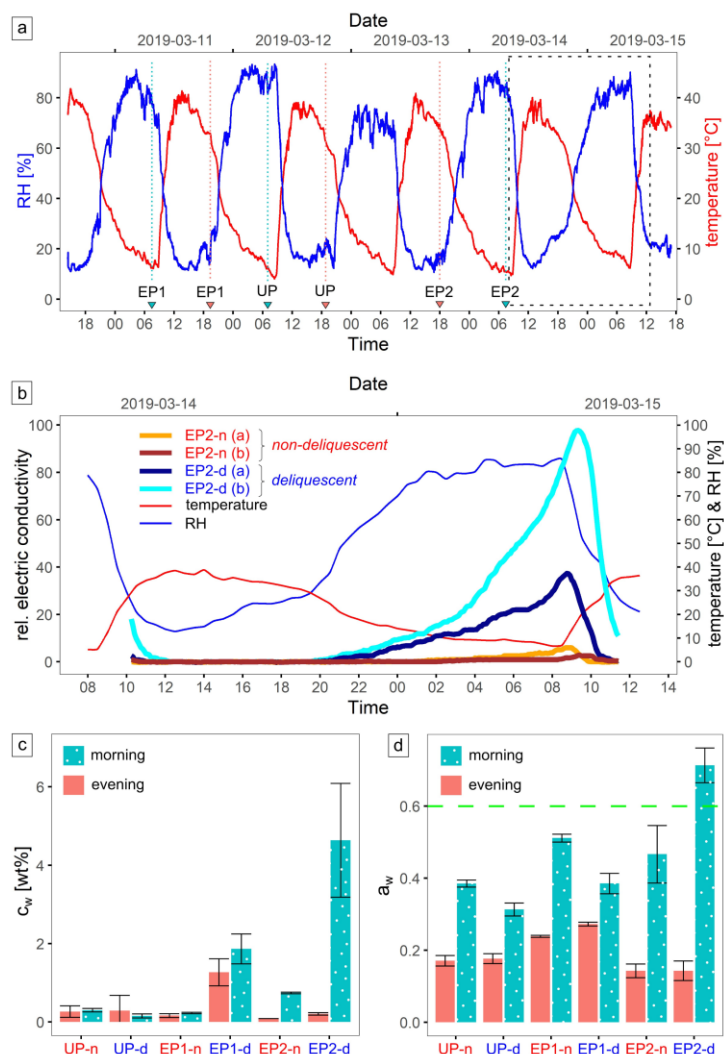
267 Soil moistening by deliquescence was observed in the morning on the surface of the polygons (EP1-d and EP2-d;
 268 “d” for deliquescent”), as well as on isolated patches of sand wedge surfaces within uneroded polygonal soils (UP-
 269 d), surrounded by otherwise dry surfaces (UP-n, EP1-n, EP2-n; “n” for non-deliquescent”) (Fig. 3).



270
 271 Figure 3: Aerial photos of the study sites during the evening and the morning that were corrected by color calibration chart. At
 272 UP darker areas in the morning occurred sporadically on the surface of the sand wedges. At the eroded polygon sites the surface
 273 of the polygons is darker in the morning, at EP1 uniform and at EP2 especially the elevated domes and crusts (Fig. 2c).

274 The ambient conditions in the study area are strongly determined by the diurnal cycle (Fig. 4a). During the night,
 275 RH reached 90 % and air temperature dropped to 5 °C, while during the day, RH decreased to 10 % with air
 276 temperature increasing to 40 °C during the field campaign, which was very similar to the two-year recording at a
 277 near-by site ranging from -4.7 – 42.7 °C and 4.4 – 97.9 % RH (Fig. 1C reference site 1). The *in situ* soil electrical
 278 conductivity ($EC_{in situ}$) is a function of salinity and moisture and measurements over time can indicate moistening
 279 and desiccation of the soil. At EP2-d during 14th and 15th of March 2019, $EC_{in situ}$ gradually increased during the
 280 night, indicating brine formation, and decreased rapidly after sunrise, indicating soil desiccation. In contrast, the
 281 sensors at EP2-n continuously detected low $EC_{in situ}$ (Fig. 4b), but also measured a minor increase during the
 282 morning, which can indicate the formation of morning dew. Moisture was observed down to ~5 cm depth, and
 283 below the soil remained dry. The water activity (a_w) remained generally low with $a_w < 0.5$ except for the EP2-d in
 284 the morning (7:30 local time), with $a_w = 0.71$ (Fig. 4c). Here, water content was most elevated, highlighting the
 285 high deliquescence potential of this site. In the EP1-d, the water uptake during the night was not as prominent.
 286 Moreover, the water content in the evening sample (19:30 local time) remained elevated. This suggests the
 287 presence of hydrated minerals like mirabilite which can dehydrate during the drying process at 60 °C. However,
 288 these were not found with X-ray diffraction (XRD). At the UP-d site, no significant water uptake could be detected
 289 with the applied method (Fig. 4d).

Deleted:

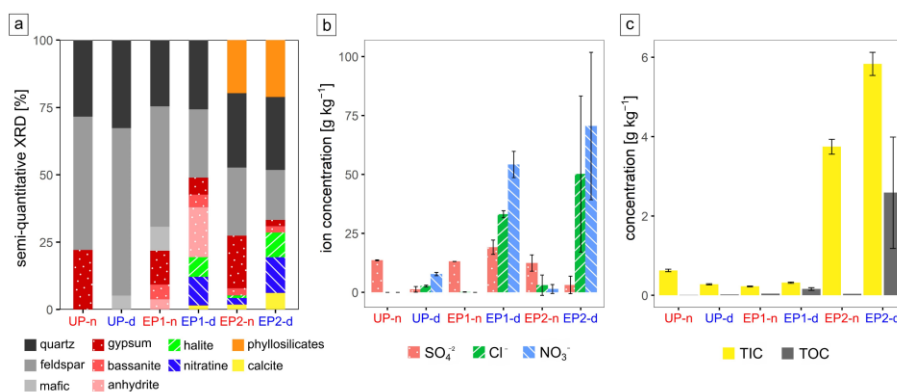


291
 292 Figure 4: Environmental monitoring data. a) Air temperature and relative humidity (RH) in the study area recorded during the
 293 sampling campaign with the sampling time (local time UTC-3 h), marked by blue triangles (morning) and red triangles
 294 (evening), and the zoom-in area (dashed box) for b). b) Relative electric conductivity ($EC_{in\ situ}$) of the surface (0-5 cm depth)
 295 at EP2 site for a day cycle. The deviation between the replicate measurement can be manifold, either by different salt
 296 composition or texture of the soil in the measurement volume or by poor electrode contact. c) Water content (c_w) and d) water
 297 activity (a_w) for each sample site in the evening (18:00) and in the morning (7:30). The green dashed line is the limit for
 298 microbial activity (Stevenson et al., 2015). Uncertainties derived from triplicate samples.

299 For the geochemical analysis the samples taken during the morning were selected. The XRD and ion
 300 chromatography (IC) analysis revealed that samples, which experienced intense deliquescence (EP1-d and EP2-
 301 d), contain up to 50 g kg^{-1} chlorides in the form of halite (NaCl) and up to 110 g kg^{-1} nitrates in the form of
 302 nitrate (NaNO_3) (Fig. 5a, b). In the samples from UP-d with minor and isolated deliquescence spots, XRD did
 303 not detect any salts, but the more sensitive IC detected low concentrations of nitrate (8 g kg^{-1}) and chloride (3
 304 g kg^{-1}). The non-deliquescence sites (UP-n, EP1-n, EP2-n) are dominated by sulfates, mainly gypsum

305 (CaSO₄×2H₂O) and minor amounts of anhydrite (CaSO₄) or bassanite (CaSO₄×0.5H₂O). In the deliquescent soils,
 306 gypsum, anhydrite, and bassanite have also been detected, but in lower quantities. The quantity of sulfates is better
 307 represented in the semi-quantitative XRD data; as for the IC analysis, samples were leached with a 1:10 (soil to
 308 water) ratio, being unable to dissolve entirely calcium sulfate (water solubility ~2 g L⁻¹) (Fig. 5a, b). The sand
 309 wedges at UP are salt poor, however, they contain small amounts of chloride and nitrate up to 10 g kg⁻¹. Besides
 310 the salts, EP2 samples, especially EP2-d, contained detectable amounts of phyllosilicates and calcite (Fig. 5a).

311 Elemental analysis of nitrogen (N) and sulfur (S) for the EP2 samples supports the XRD results, showing nitrogen
 312 enrichment in the EP2-d samples and levels close to the detection limit (0.1 g kg⁻¹) in the EP2-n samples. In
 313 contrast, these samples are more concentrated in sulfur while the deliquescent samples (EP2-d) have comparably
 314 low levels (Fig. S2). Carbon (C) is found in the soil as organic matter and as carbonate, given as total organic
 315 carbon (TOC) and total inorganic carbon (TIC), respectively (Fig. 5c). TIC is most concentrated in the EP2
 316 samples, with up to 5.8 g kg⁻¹, while TOC can be detected where deliquescence was observed predominantly (EP2-
 317 d & EP1-d), reaching values of up to 3.7 g kg⁻¹. In the surrounding soils, organic carbon was below the detection
 318 limit (0.1 g kg⁻¹).

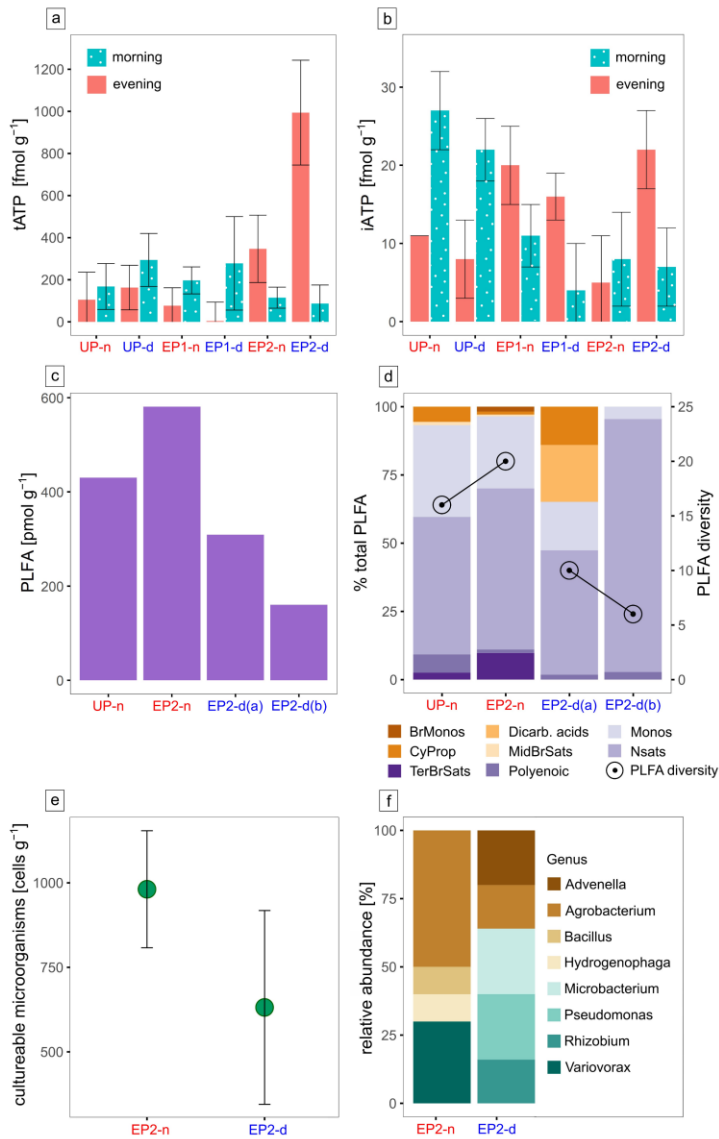


319 Figure 5: Geochemical data. A) semi-quantitative mineralogical composition by XRD of bulk samples. B) Concentration of
 320 the main water-soluble anions. C) Total carbon concentration shown as total organic carbon (TOC) and total inorganic carbon
 321 (TIC). Uncertainties derived from triplicate samples.
 322

323 The collected biological data is overall very sparse, reflecting the harsh conditions in this extreme environment.
 324 Adenosine triphosphate (ATP) is the ubiquitously used energy source by life and can be utilized as an indicator of
 325 microbial activity (Blagodatskaya and Kuzyakov, 2013). The total ATP concentrations (tATP) in our samples were
 326 extremely low, with values of 1 pmol g⁻¹ sediment or even lower, reflecting the extreme conditions for life in the
 327 Atacama Desert (Fig. 6a). The intracellular ATP (iATP), extracted from intact cells, is only a small fraction of the
 328 tATP and is overall lower in the deliquescent soils compared to the surrounding non-deliquescent soils (Fig. 6b).
 329 Significant turnover rates during the morning and evening are not visible.

330 The following biological analyses were employed on the samples which were sampled in the morning.
 331 Phospholipid fatty acids (PLFA) are indicative for soil habitability and cell viability as they are the main
 332 components of bacterial membranes that can easily degrade after cell death (Connon et al., 2007). Additionally,
 333 they can be used to analyze the general microbial community on a broad taxonomic level (Mangelsdorf et al.,
 334 2020). For comparison between the deliquescent and non-deliquescent surfaces, two replicate samples from EP2-
 335 d (EP2-d a, EP2-d b) and from EP2-n and UP-n one sample each were selected for PLFA analysis. PLFAs were
 336 found in all investigated samples with concentrations above the blank (37 pmol g⁻¹). The deliquescent soils with
 337 nitrate and chloride salts contained less PLFAs (160–308 pmol g⁻¹) than the non-deliquescent sulfate-cemented
 338 soils (430–581 pmol g⁻¹) (Fig. 6c). This trend has also been found in the PLFA diversity, where the deliquescent
 339 samples have 6 and 10 different PLFAs compared to 15 and 20 in the non-deliquescent samples (Fig. 6d). In the
 340 overall inventory, the normal saturated (58 %) and the monoenoic fatty acids (24 %) were most abundant and were
 341 found together with the polyenoic fatty acids (3 %) in all samples. The terminally branched saturated acids were
 342 found in the low saline, non-deliquescent UP-n and EP2-n samples and the dicarboxylic fatty acids, known for
 343 *Acidobacteria* membrane, are exclusively detected in the high saline, deliquescent EP2-d samples.

344 The cultivation experiments conducted with the EP2 samples yielded colony forming unit (CFU) counts in the
 345 order of 10^2 – 10^3 cells g^{-1} soil (Fig. 6e). The CFU values of EP2-d are on average lower compared to the EP2-n
 346 samples, indicating lower bacterial abundance in the deliquescent soils. Additionally, 16S rRNA gene sequencing
 347 was performed on individual colonies identifying eight different genera in the surface soil, five in EP2-d samples
 348 and four in EP2-n samples. Bacteria of the genus *Advevella*, *Microbacterium*, *Pseudomonas* and *Rhizobium* were
 349 found exclusively in the EP2-d, and the genus *Bacillus*, *Hydrogenophaga* and *Variovorax* exclusively in EP2-n
 350 (Fig. 6f, Table S1).

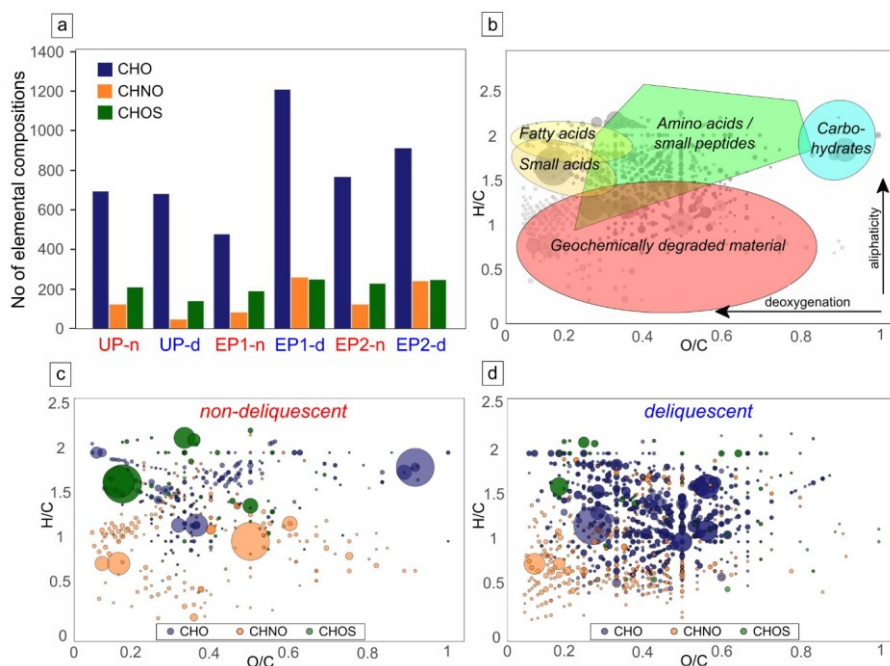


351
 352 Figure 6: Microbial life and activity data. ATP concentration at all sampling sites during morning and evening hours split in a)
 353 total ATP (tATP) and b) intracellular ATP (iATP) concentration. c) PLFA concentration. d) The relative abundance of different
 354 PLFA groups including branched monoenoic (BrMonos), dicarboxylic acids (dicarb. acids), monoenoic (Monos), cyclopropyl

355 (CyProp), mid-chain branched saturated (MidBrSats), terminally branched saturated (TerBrSats), normal saturated (Nsats) and
 356 polyenoic fatty acids, as well as the PLFA diversity (number of different PLFA). e) Dot plot of the cultivation experiment data
 357 with colony forming units (CFUs) per sample weight, uncertainties derive from sample triplicates. f) 16S rRNA sequences of
 358 the cultivated microbes on genus level. PLFA analysis and culturing experiments were focused on the EP2 site where most
 359 intense deliquescence occurred.

360 Culture-independent 16S rRNA gene PCR amplicon sequencing using the bulk soil sample was challenging due
 361 to very low DNA concentration resulting from low microbial abundance, which prevented a statistically significant
 362 distinction between deliquescent and non-deliquescent soils. The alpha diversity is slightly higher for the
 363 deliquescent samples which supports the cultivation experiment results (Fig. S3), but the canonical analysis of
 364 principal coordinates is inconclusive (Fig. S4).

365 To gain a more comprehensive understanding of the increased organic matter in the deliquescent samples and to
 366 compare it with the non-deliquescent samples, organic molecules were measured via direct injection electrospray
 367 ionization Fourier transform ion cyclotron resonance mass spectrometry (ESI(-) FT-ICR-MS). Each mass signal
 368 was assigned to its corresponding molecular composition and classified as CHO, CHOS, or CHNO species. The
 369 comparison of uneroded and eroded soils differs in terms of the number of annotated elemental compositions. The
 370 results show a higher abundance of CHO and CHNO molecular features is found in the intense deliquescence soil
 371 surface of the eroded polygon sites (EP1-d, EP2-d) (Fig. 7a).



372
 373 Figure 7: Compositional profiles of organic matter. a) Abundance of elemental compositions in uneroded and eroded polygon
 374 sites. b) Exemplary van Krevelen diagram plotting the hydrogen to carbon atomic ratio (H/C) as a function of the oxygen to
 375 carbon (O/C) atomic ratio of organic compounds. The positions of chemical classes (colored areas) are depicted in
 376 compositional space. Highly aliphatic compounds are mostly presented in the upper (H/C ratio > 1) and aromatic compounds
 377 in the lower area (H/C ratio < 1). c) Molecular compositions specific for non-deliquescent surfaces and d) for deliquescent,
 378 nitrate-rich surfaces are plotted as CHO (blue), CHOS (green), and CHNO (orange), and bubble sizes depict mass signal
 379 intensities.

380 The relationship between the atomic ratio O/C vs. H/C of the assigned molecules is plotted in the van Krevelen
 381 diagrams (Fig. 7b-d, S5). The results revealed a broad distribution within the compositional space reflecting the
 382 complexity of the organic molecules contained in the samples encompassing possible amino acids, small peptides,
 383 and phenolic compounds. The dominance of phenolic compounds reflects an overall geochemical signature,
 384 indicating low bioactivity and long-term geochemical processes responsible for lignin-like organic matter

385 degradation. Profiling the mass signal intensities across the entire spectrum reveal a differentiation of samples into
386 two groups: non-deliqescent soils show only minor specific molecules with few intense CHOS signals (Fig. 7c),
387 whereas deliquescent soils with additional chlorides and nitrates (especially from EP1 and EP2 sites) have more
388 specific CHO and CHNO molecules (Fig. 7d).

389 4 DISCUSSION

390 4.1 Deliquescence-driven environment

391 The investigated sites are located on alluvial fan deposits of Miocene to Pliocene age (Sernageomin and others,
392 2003; Amundson et al., 2012). During millions of years of hyperaridity large amounts of atmospherically derived
393 salts, including nitrates, were added by dry deposition (Ericksen, 1981; Michalski et al., 2004; Ewing et al., 2006).
394 Although erosion is generally minimal in the Atacama Desert, in few locations, vulnerable to eolian erosion, the
395 upper soil layers have been removed (Sager et al., 2022). This erosion was evident at the EP sites, indicated by the
396 highly soluble salts and the anhydrite at the surface of the polygons, both found otherwise in the subsurface below
397 40 cm depth of the uneroded soils (Schulze-Makuch et al., 2018; Arens et al., 2021; Sager et al., 2021). Local
398 morphology and topography did not indicate a connection to active fluvial channels (Fig. S1). However, the
399 erosional surfaces tend to correlate with topographic lows, such as ancient channels and the valley basin (Fig. 1b).
400 These ancient morphological features have been shown to influence soil composition and structures subsequently
401 impacting the vulnerability of the soil surface to eolian erosion (Pfeiffer et al., 2021; Sager et al., 2022).

402 Due to this erosion, the exposed hygroscopic nitrate- and chloride-salts interact with occurring rain, fog, and even
403 increased air humidity. Generally, minimal precipitation occurs only once every few years (McKay et al., 2003;
404 Bozkurt et al., 2016). In contrast, air humidity fluctuates diurnally from values as low as 5 % RH during the day,
405 to high values reaching saturation during the night due to strong temperature fluctuations. This can also lead to fog
406 formation. Normally, the dew point on the surface is not reached solely by a drop in temperature (McKay et al.,
407 2003), but also due to the presence of hygroscopic salts that enable deliquescence, providing liquid water even at
408 RH >75 % for halite and >74 % of nitrate at 20 °C (Greenspan, 1977). For eutectic NaCl-NaNO₃ mixture
409 deliquescence occurs even at 67 % RH (Tang and Munkelwitz, 1994; Gupta et al., 2015).

410 The repeated cycles of moistening and evaporation of the hygroscopic soil patches can create efflorescence
411 structures, like soil doming and encrustation of salt-rich sediment (Sager et al., 2022), which are also observed at
412 the EP2 site. The absence of the efflorescence at the EP1 site correlates with the lower water uptake of the soil,
413 while the salt content is similar (Fig 3,4). This suggests salt exposure at EP1 may have occurred more recently and
414 that the secondary processes have not yet caused measurable effects. Additionally, the increased moisture uptake
415 of EP2-d compared to EP1-d suggests that the surface morphology has an impact on the deliquescence. Possibly,
416 due to the efflorescence structures (Fig. 2) the soil surface may cool down more efficiently, lowering the dew
417 point.

418 The ongoing process of deliquescence and efflorescence of the surface at EP2 could also be responsible for the
419 higher abundance of phyllosilicates and carbonates compared to EP1. These may have accumulated through the
420 entrapment of eolian dust, sticking to the moist soil surface and incorporated into the salt crust. Alternatively, the
421 phyllosilicates and carbonate can have formed autochthonously due to more frequent presence of water in these
422 soil patches resulting in enhanced aqueous weathering (Ewing et al., 2006).

423 4.2 Habitability of the salt crust

424 With the common notion "follow the water" in searching for life, the repeated occurrence of soil moisture was a
425 strong indicator of a new potential micro-habitat in the hyperarid Atacama Desert. The environmental monitoring
426 and the geochemical results confirmed the initial observation in the field that the soil surfaces can provide moisture,
427 which is potentially suitable for microbial activity (Stevenson et al., 2015). Deliquescence prolongs the presence
428 of liquid water, making microbial activity more likely. This is crucial, considering that moisture, mainly brought
429 into the Yungay valley by humid air from the Pacific Ocean, is only sufficient to yield ~400 h per year with dew
430 formation (>95 % RH) (Warren-Rhodes et al., 2006). Extrapolating the observed deliquescence during the
431 sampling campaign (with RH >85 %) and the recording of air humidity over two years, the duration of moist soil
432 is ~10 times longer compared to surfaces with no hygroscopic salts.

433 However, our microbiological analysis did not support an enhanced habitability for microorganisms of the
434 investigated soils. In contrast, the results showed even lower microbial activity and microbial growth compared to
435 the control samples with no observed deliquescence and no or minor amounts of hygroscopic salts (Fig. 3, 5a). For
436 the cell cultivation experiments a low salinity growth medium was used, which could have favored the growth of
437 microorganisms in the non-deliqescent soil samples or could have suppressed halophilic organisms. For future
438 investigations, additional experiments with more saline growth media could help to verify this trend. The genetic
439 data of the cultivated bacteria indicates that these are native organisms known from the Atacama Desert
440 specifically in the Yungay valley (Navarro-Gonzalez et al., 2003; Azua-Bustos et al., 2019; Azua-Bustos et al.,
441 2020). On the other hand, the plant-symbiotic genus *Rhizobium* found in the deliquescent soil samples is unlikely
442 to thrive in the unvegetated study area (Araya et al., 2020). This and the lower bacterial abundance but higher
443 alpha-diversity in the deliquescent samples may suggest that the deposition of airborne input of microorganisms is
444 promoted by enhanced adhesion of moist soil surfaces.

445 Previous studies investigated non-deliqescent soils in the hyperarid region regarding their biological activity and
446 diversity showing similar results to the here investigated non-deliqescent soils (Connon et al., 2007; Lester et al.,
447 2007; Crits-Christoph et al., 2013; Schulze-Makuch et al., 2018; Warren-Rhodes et al., 2019; Knief et al., 2020;
448 Shen, 2020; Sager et al., 2023). Also, metabolic signatures match, showing a geochemical footprint, superimposed
449 by fresh organic material indicating at least some metabolic activity (Schulze-Makuch et al., 2018). Microhabitats
450 previously studied and most related to the here investigated deliquescent soils are halite nodules within salars,
451 which also undergo diurnal deliquescence (Wierzchos et al., 2006; Robinson et al., 2015; Valea, 2015; Schulze-
452 Makuch et al., 2021; Perez-Fernandez et al., 2022). Spatially closest examples can be found in the Aguas Blancas
453 Salar, 10 km east of the sample site. Besides microscopic confirmation of intact microorganisms, these niches
454 show higher PLFA concentration and diversity (Ziolkowski et al., 2013; Schulze-Makuch et al., 2021), as well as
455 metabolic composition reflecting fresh biological material and microbial activity (Schulze-Makuch et al., 2021).

456 Comparing the sulfate-rich shallow subsurface and halite nodules with our nitrate-rich salt crust the most striking
457 difference is the nitrate abundance in the here investigated salt crusts. To our knowledge, only endolithic
458 communities have been reported in salt crusts containing halite or gypsum (Wierzchos et al., 2006; Wierzchos et
459 al., 2011).

460 The reduced habitability of the nitrate crusts can have multiple reasons. Potential organisms thriving in the formed
461 brine saturated with NaNO_3 would be confronted with higher osmotic stress, due to high solubility of NaNO_3 .
462 Additionally, nitrate induces chaotropic stress affecting the bio-macromolecular structure (Lima Alves et al.,
463 2015). This characteristic correlates in large parts with the Hofmeister series giving the order of effectiveness of
464 protein precipitation as follows: $\text{SO}_4^{2-} < \text{Cl}^- < \text{NO}_3^- < \text{ClO}_4^-$ (Hyde et al., 2017). While microbial growth could
465 not be detected yet in NaNO_3 solutions with concentrations exceeding 34 wt% (4.9 M) (Heinz et al., 2021), the
466 brine formed by deliquescence would have an initial concentration of 10.9 M (i.e. saturation point at 25 °C)
467 (Archer, 2000). Nitrates can also induce reactive oxygen species (ROS, e.g., OH^- , H_2O_2) or reactive nitrogen
468 species (RNS, e.g., NO^\bullet , NO_2^-) which cause oxidative and nitrosative stress (Ansari et al., 2015). This can occur
469 in the presence of UV radiation, which is intense in the high-altitude and cloud-free Atacama Desert reducing
470 nitrate to nitrite and OH^- , or NO^\bullet and O_2^{2-} (Yang et al., 2021).

471 The nitrate-rich efflorescence crusts create an extremely rare environment. Sand wedge polygonal grounds are
472 widely found in the Yungay valley and within the hyperarid core of the Atacama Desert (Eriksen, 1981; Sager et
473 al., 2021). However, due to the hyperarid condition, erosion is minimal which is why these erosional surfaces are
474 scarce. Despite the hyperaridity, the nitrate crust is presumably not stable at the surface, as precipitation is
475 eventually washing the salts on the alluvial fan down into the subsurface or is eroded by the wind. Hence, the
476 occurrence of nitrate-rich environments is likely so rare throughout Earth history that life has not evolved any
477 strategies for adaptation to cope with these exceptionally harsh conditions.

478 4.3 Preservation of biomolecules

479 The here measured biological and biogeochemical parameters indicate that habitability is reduced in the nitrate-
480 rich soil crusts. However, organic carbon is elevated in comparison to the surrounding soil as well as compared to
481 previous studies (Connon et al., 2007; Lester et al., 2007). This is also indicated by the composition of organic
482 matter, which was more diverse at the nitrate-rich sites. The uneroded caliche layer residing at depth, being the
483 precursor of the deliquescent surfaces, does not show such an abundance and diversity of organic carbon (Fuentes
484 et al., 2021; Schulze-Makuch et al., 2021). Thus, carbon compounds have been presumably introduced after

485 exposure to the atmosphere. As proposed for the phyllosilicates and carbonates (Sager et al., 2022), also organic
486 carbon could be trapped by the moist salt crusts in the form of airborne dust, including microbes or already
487 degraded organic matter. Potential sources for the organic matter could be the sea spray from the Pacific Ocean
488 transported by the dominating west wind (McKay et al., 2003; Azua-Bustos et al., 2019). Also, fog oasis and sparse
489 plant cover in the coastal range could be potential sources for more organic-rich dust particles (Quade et al., 2007).
490 Salts are recognized for their role in stabilizing biomarkers. Hypersaline environments often exhibit enhancements
491 of particular molecular biomarkers, such as gammacerane (Damsté et al., 1995), or a higher ratio of acidic to basic
492 amino acids (Rhodes et al., 2010) and lead to entrapment of biogenic molecules (Cockell et al., 2020) and microbes
493 (Perl and Baxter, 2020). Nitrate salts are known to inhibit microbial activity and have been used to cure food,
494 especially meat (Majou and Christieans, 2018). Besides higher dust (including organic matter through organic
495 aerosol dry deposition) accumulation rates, biological degradation could also be hindered in the same way by the
496 presence of nitrates, leading to higher TOC values in the here investigated nitrate-rich soil crusts. Nitrate-rich
497 subsurface layers within million-year-old hypersaline deposits of the Atacama Desert revealed a variety of
498 biomolecules, confirming the high biosignature preservation potential of nitrates (Fernández-Remolar et al., 2013).

499 Besides these benefits for biomass preservation, ROS or RNS originating from UV-exposed nitrates as discussed
500 earlier, can enhance geochemical degradation of biomolecules. Indications can be found in the profiles of organic
501 matter, where small CHNO species dominate across the nitrate crusts pointing to a geochemical breakdown of
502 organic molecules with reactive nitrogen species. However, in comparison to the surrounding non-deliquescent
503 soil surfaces, the nitrate-rich soils seem to promote the preservation of organic matter.

504 4.4 Indications for the search for life on Mars

505 In addition to abundant sulfate and chloride deposits also nitrates have been detected on Mars e.g., by Curiosity
506 Rover in the Gale Crater at concentrations up to 600 mg kg⁻¹ (Stern et al., 2015; Stern et al., 2017). Morphological
507 and geochemical indicators suggests that during the Hesperian and early Amazonian periods environmental
508 conditions like the water availability on Mars has been comparable to the contemporary Atacama Desert (Stepinski
509 and Stepinski, 2005; Bibring et al., 2006). It is plausible that like in the Atacama Desert, also on Mars the
510 accumulation of nitrates was dominated by dry fallout from the atmosphere, produced by volcanic lightning and
511 impacts during the first 1 Ga of Mars history (Michalski et al., 2004; Segura and Navarro-González, 2005;
512 Manning et al., 2009). Analogous to the Atacama Desert, nitrate deposits could have formed in the Martian
513 subsurface during that time. Extrapolating our findings to Mars would make nitrates-rich soils as a potential habitat
514 unfavorable, but due to the enhanced preservation of biomolecules these are still a promising target for finding
515 relics of ancient Martian life. This is also indicated by the detection of biomolecules in a million-year-old nitrate-
516 rich deposit in the Atacama Desert (Fernández-Remolar et al., 2013). The habitability of Martian nitrate-rich crust
517 should not be ruled out, since the evolutionary pressure on Mars could have enabled microbes to adapt to high
518 nitrate concentrations, as life on Earth has adapted thrive in brines containing the most abundant salt, being NaCl
519 (Heinz et al., 2019). Due to the gradual and global expansion of hyperarid conditions on Mars, putative life could
520 have evolved strategies to adapt to high salt concentrations, including nitrates, and by making use of their
521 hygroscopic nature (Davila and Schulze-Makuch, 2016; Maus et al., 2020). Maybe even more important on Mars,
522 these nitrate deposits could also represent a rare nitrogen-source for life as we know it, to build biomolecules like
523 amino acids and nucleobases.

524 5 CONCLUSION

525 Our investigation of the deliquescence of nitrate-rich soils in the Atacama Desert provides new insights into the
526 dynamics and the habitability in one of the Earth's most extreme environments. Despite providing transient
527 moisture, our results indicate that the nitrate-rich surfaces exhibit lower microbial abundance and activities
528 compared to the surrounding non-deliquescent surfaces. The high nitrate concentrations appear to suppress
529 microbial activity, likely due to osmotic and chaotropic stress and the potential production of reactive nitrogen
530 species. Remarkably, the nitrate-rich soil surfaces bear elevated geochemically degraded organic matter, indicating
531 an enhanced biomolecule preservation of these environments under such extreme conditions. These findings
532 highlight the dual role of nitrates in organic matter preservation and microbial inhibition. The inhabitability despite
533 water availability and the preservation potential in nitrate-rich soils underscores their importance in the search for
534 life in hyperarid environments on Earth and aids in the field of astrobiology to the search for life on Mars.

535 REFERENCES

- 536 Altschul, S.F., Madden, T.L., Schäffer, A.A., Zhang, J., Zhang, Z., Miller, W., Lipman, D.J., 1997. Gapped
537 BLAST and PSI-BLAST: a new generation of protein database search programs. *Nucleic acids research* 25,
538 3389–3402.
- 539 Amundson, R., Dietrich, W., Bellugi, D., Ewing, S., Nishiizumi, K., Chong, G., Owen, J., Finkel, R., Heimsath,
540 A., Stewart, B., Caffee, M., 2012. Geomorphologic evidence for the late Pliocene onset of hyperaridity in the
541 Atacama Desert. *Geological Society of America Bulletin* 124, 1048–1070.
- 542 Ansari, F.A., Ali, S.N., Mahmood, R., 2015. Sodium nitrite-induced oxidative stress causes membrane damage,
543 protein oxidation, lipid peroxidation and alters major metabolic pathways in human erythrocytes. *Toxicology*
544 *in Vitro* 29, 1878–1886.
- 545 Araya, J.P., González, M., Cardinale, M., Schnell, S., Stoll, A., 2020. Microbiome dynamics associated with the
546 Atacama flowering desert. *Frontiers in microbiology* 10, 3160.
- 547 Archer, D.G., 2000. Thermodynamic properties of the NaNO₃+H₂O system. *Journal of Physical and Chemical*
548 *Reference Data* 29, 1141–1156.
- 549 Arens, F.L., Airo, A., Feige, J., Sager, C., Wiechert, U., Schulze-Makuch, D., 2021. Geochemical proxies for
550 water-soil interactions in the hyperarid Atacama Desert, Chile. *CATENA* 206, 105531.
- 551 Artieda, O., Davila, A., Wierzchos, J., Buhler, P., Rodríguez-Ochoa, R., Pueyo, J., Ascaso, C., 2015. Surface
552 evolution of salt-encrusted playas under extreme and continued dryness. *Earth Surf. Process. Landforms* 40,
553 1939–1950.
- 554 Azua-Bustos, A., Fairén, A.G., Silva, C.G., Carrizo, D., Fernández-Martínez, M.Á., Arenas-Fajardo, C.,
555 Fernández-Sampedro, M., Gil-Lozano, C., Sánchez-García, L., Ascaso, C., Wierzchos, J., Rampe, E.B., 2020.
556 Inhabited subsurface wet smectites in the hyperarid core of the Atacama Desert as an analog for the search for
557 life on Mars. *Scientific reports* 10, 19183.
- 558 Azua-Bustos, A., González-Silva, C., Fernández-Martínez, M.Á., 2019. Aeolian transport of viable microbial life
559 across the Atacama Desert, Chile: Implications for Mars. *Scientific reports* 9, 11024.
- 560 Bibring, J.-P., Langevin, Y., Mustard, J.F., Poulet, F., Arvidson, R., Gendrin, A., Gondet, B., Mangold, N., Pinet,
561 P., Forget, F., others, 2006. Global mineralogical and aqueous Mars history derived from OMEGA/Mars
562 Express data. *Science (New York, N.Y.)* 312, 400–404.
- 563 Blagodatskaya, E., Kuzyakov, Y., 2013. Active microorganisms in soil: critical review of estimation criteria and
564 approaches. *Soil Biology and Biochemistry* 67, 192–211.
- 565 Bozkurt, D., Rondanelli, R., Garreaud, R., Arriagada, A., 2016. Impact of warmer eastern tropical Pacific SST on
566 the March 2015 Atacama floods. *Monthly Weather Review* 144, 4441–4460.
- 567 Callahan, B.J., McMurdie, P.J., Rosen, M.J., Han, A.W., Johnson, A.J.A., Holmes, S.P., 2016. DADA2: High-
568 resolution sample inference from Illumina amplicon data. *Nature methods* 13, 581–583.
- 569 Cockell, C.S., Wilhelm, M.B., Perl, S., Wadsworth, J., Payler, S., McMahon, S., Paling, S., Edwards, T., 2020.
570 0.25 Ga salt deposits preserve signatures of habitable conditions and ancient lipids. *Astrobiology* 20, 864–
571 877.
- 572 Connon, S.A., Lester, E.D., Shafaat, H.S., Obenhuber, D.C., Ponce, A., 2007. Bacterial diversity in hyperarid
573 Atacama Desert soils. *J. Geophys. Res.* 112.
- 574 Crits-Christoph, A., Robinson, C.K., Barnum, T., Fricke, W.F., Davila, A.F., Jedynek, B., McKay, C.P.,
575 DiRuggiero, J., 2013. Colonization patterns of soil microbial communities in the Atacama Desert. *Microbiome*
576 1, 1–13.
- 577 Damsté, J.S.S., Kenig, F., Koopmans, M.P., Köster, J., Schouten, S., Hayes, J.M., Leeuw, J.W. de, 1995. Evidence
578 for gammacerane as an indicator of water column stratification. *Geochimica et Cosmochimica Acta* 59, 1895–
579 1900.
- 580 Davila, A.F., Hawes, I., Ascaso, C., Wierzchos, J., 2013. Salt deliquescence drives photosynthesis in the hyperarid
581 Atacama Desert. *Environmental microbiology reports* 5, 583–587.
- 582 Davila, A.F., Schulze-Makuch, D., 2016. The Last Possible Outposts for Life on Mars. *Astrobiology* 16, 159–168.
- 583 Dunai, T.J., González L., G., Juez-Larré, J., 2005. Oligocene–Miocene age of aridity in the Atacama Desert
584 revealed by exposure dating of erosion-sensitive landforms. *Geology* 33, 321–324.
- 585 Ericksen, G.E., 1981. Geology and Origin of nitrate deposition in Atacama Desert. *Geological Society of America*
586 *Bulletin*.

587 Ewing, S.A., Sutter, B., Owen, J., Nishiizumi, K., Sharp, W., Cliff, S.S., Perry, K., Dietrich, W., McKay, C.P.,
588 Amundson, R., 2006. A threshold in soil formation at Earth's arid-hyperarid transition. *Geochimica et*
589 *Cosmochimica Acta* 70, 5293–5322.

590 Ewing, S.A., Yang, W., DePaolo, D.J., Michalski, G., Kendall, C., Stewart, B.W., Thiemens, M., Amundson, R.,
591 2008. Non-biological fractionation of stable Ca isotopes in soils of the Atacama Desert, Chile. *Geochimica et*
592 *Cosmochimica Acta* 72, 1096–1110.

593 Fernández-Remolar, D.C., Chong-Díaz, G., Ruíz-Bermejo, M., Harir, M., Schmitt-Kopplin, P., Tziotis, D.,
594 Gómez-Ortiz, D., García-Villadangos, M., Martín-Redondo, M.P., Gómez, F., Rodríguez-Manfredi, J.A.,
595 Moreno-Paz, M., Diego-Castilla, G. de, Echeverría, A., Urtuvia, V.N., Blanco, Y., Rivas, L., Izawa, M.R.M.,
596 Banerjee, N.R., Demergasso, C., Parro, V., 2013. Molecular preservation in halite- and perchlorate-rich
597 hypersaline subsurface deposits in the Salar Grande basin (Atacama Desert, Chile): Implications for the search
598 for molecular biomarkers on Mars. *J. Geophys. Res. Biogeosci.* 118, 922–939.

599 Fuentes, B., Choque, A., Gómez, F., Alarcón, J., Castro-Nallar, E., Arenas, F., Contreras, D., Mörchen, R.,
600 Amelung, W., Knief, C., Moradi, G., Klumpp, E., Saavedra, C.P., Prietzel, J., Klysubun, W., Remonsellez, F.,
601 Bol, R., 2021. Influence of Physical-Chemical Soil Parameters on Microbiota Composition and Diversity in a
602 Deep Hyperarid Core of the Atacama Desert. *Frontiers in microbiology* 12, 794743.

603 Greenspan, L., 1977. Humidity fixed points of binary saturated aqueous solutions. *Journal of research of the*
604 *National Bureau of Standards. Section A, Physics and chemistry* 81, 89.

605 Gupta, D., Kim, H., Park, G., Li, X., Eom, H.-J., Ro, C.-U., 2015. Hygroscopic properties of NaCl and NaNO₂;
606 mixture particles as reacted inorganic sea-salt aerosol surrogates. *Atmos. Chem. Phys.* 15, 3379–3393.

607 Heinz, J., Rambags, V., Schulze-Makuch, D., 2021. Physicochemical Parameters Limiting Growth of
608 *Debaryomyces hansenii* in Solutions of Hygroscopic Compounds and Their Effects on the Habitability of
609 *Martian Brines. Life (Basel, Switzerland)* 11.

610 Heinz, J., Waajen, A.C., Airo, A., Alibrandi, A., Schirmack, J., Schulze-Makuch, D., 2019. Bacterial Growth in
611 Chloride and Perchlorate Brines: Halotolerances and Salt Stress Responses of *Planococcus halocryophilus*.
612 *Astrobiology* 19, 1377–1387.

613 Hwang, Y., Schulze-Makuch, D., Arens, F.L., Saenz, J.S., Adam, P.S., Sager, C., Bornemann, T.L.V., Zhao, W.,
614 Zhang, Y., Airo, A., Schloter, M., Probst, A.J., 2021. Leave no stone unturned: individually adapted
615 xerotolerant *Thaumarchaeota* sheltered below the boulders of the Atacama Desert hyperarid core. *Microbiome*
616 9, 234.

617 Hyde, A.M., Zultanski, S.L., Waldman, J.H., Zhong, Y.-L., Shevlin, M., Peng, F., 2017. General principles and
618 strategies for salting-out informed by the Hofmeister series. *Organic Process Research & Development* 21,
619 1355–1370.

620 Jordan, T.E., Kirk-Lawlor, N.E., Blanco, N.P., Rech, J.A., Cosentino, N.J., 2014. Landscape modification in
621 response to repeated onset of hyperarid paleoclimate states since 14 Ma, Atacama Desert, Chile. *Bulletin* 126,
622 1016–1046.

623 Knief, C., Bol, R., Amelung, W., Kusch, S., Frindte, K., Eckmeier, E., Jaeschke, A., Dunai, T., Fuentes, B.,
624 Mörchen, R., Schütte, T., Lücke, A., Klumpp, E., Kaiser, K., Rethemeyer, J., 2020. Tracing elevational
625 changes in microbial life and organic carbon sources in soils of the Atacama Desert. *Global and Planetary*
626 *Change* 184, 103078.

627 Lester, E.D., Satomi, M., Ponce, A., 2007. Microflora of extreme arid Atacama Desert soils. *Soil Biology and*
628 *Biochemistry* 39, 704–708.

629 Lima Alves, F. de, Stevenson, A., Baxter, E., Gillion, J.L.M., Hejazi, F., Hayes, S., Morrison, I.E.G., Prior, B.A.,
630 McGenity, T.J., Rangel, D.E.N., others, 2015. Concomitant osmotic and chaotropicity-induced stresses in
631 *Aspergillus wentii*: compatible solutes determine the biotic window. *Current Genetics* 61, 457–477.

632 Majou, D., Christeans, S., 2018. Mechanisms of the bactericidal effects of nitrate and nitrite in cured meats. *Meat*
633 *Science* 145, 273–284.

634 Mangelsdorf, K., Karger, C., Zink, K.-G., 2020. Phospholipids as life markers in geological habitats.
635 *Hydrocarbons, oils and lipids: diversity, origin, chemistry and fate*, 445–473.

636 Manning, C.V., Zahnle, K.J., McKay, C.P., 2009. Impact processing of nitrogen on early Mars. *Icarus* 199, 273–
637 285.

638 Martin, M., 2011. Cutadapt removes adapter sequences from high-throughput sequencing reads. *EMBnet.journal*
639 17.

640 Maus, D., Heinz, J., Schirmack, J., Airo, A., Kounaves, S.P., Wagner, D., Schulze-Makuch, D., 2020.
641 Methanogenic archaea can produce methane in deliquescence-driven Mars analog environments. *Scientific*
642 *reports* 10, 6.

643 McKay, C.P., Friedmann, E.I., Gómez-Silva, B., Cáceres-Villanueva, L., Andersen, D.T., Landheim, R., 2003.
644 Temperature and moisture conditions for life in the extreme arid region of the Atacama Desert: four years of
645 observations including the El Niño of 1997-1998. *Astrobiology* 3, 393–406.

646 McMurdie, P.J., Holmes, S., 2013. phyloseq: an R package for reproducible interactive analysis and graphics of
647 microbiome census data. *PloS one* 8, e61217.

648 Michalski, G., Böhlke, J.K., Thiemens, M., 2004. Long term atmospheric deposition as the source of nitrate and
649 other salts in the Atacama Desert, Chile: New evidence from mass-independent oxygen isotopic compositions.
650 *Geochimica et Cosmochimica Acta* 68, 4023–4038.

651 Mitra, S., Förster-Fromme, K., Damms-Machado, A., Scheurenbrand, T., Biskup, S., Huson, D.H., Bischoff, S.C.,
652 2013. Analysis of the intestinal microbiota using SOLiD 16S rRNA gene sequencing and SOLiD shotgun
653 sequencing. *BMC genomics* 14, 1–11.

654 Müller, K.-D., Husmann, H., Nalik, H.P., 1990. A new and rapid method for the assay of bacterial fatty acids using
655 high resolution capillary gas chromatography and trimethylsulfonium hydroxide. *Zentralblatt für*
656 *Bakteriologie* 274, 174–182.

657 Navarro-Gonzalez, R., Rainey, F., Molina, P., Bagaley, D., Hollen, B., Rosa, J., Small, A., Quinn, R., Grunthaner,
658 F., Cáceres, L., Gomez-Silva, B., McKay, C., 2003. Mars-Like Soils in the Atacama Desert, Chile, and the
659 Dry Limit of Microbial Life. *Science (New York, N.Y.)* 302, 1018–1021.

660 Nercessian, O., Noyes, E., Kalyuzhnaya, M.G., Lidstrom, M.E., Chistoserdova, L., 2005. Bacterial populations
661 active in metabolism of C1 compounds in the sediment of Lake Washington, a freshwater lake. *Applied and*
662 *environmental microbiology* 71, 6885–6899.

663 Neubauer, D., Kolmakova, O., Woodhouse, J., Taube, R., Mangelsdorf, K., Gladyshev, M., Premke, K., Grossart,
664 H.-P., 2021. Zooplankton carcasses stimulate microbial turnover of allochthonous particulate organic matter.
665 *The ISME journal* 15, 1735–1750.

666 Perez-Fernandez, C.A., Wilburn, P., Davila, A., DiRuggiero, J., 2022. Adaptations of endolithic communities to
667 abrupt environmental changes in a hyper-arid desert. *Scientific reports* 12, 20022.

668 Perl, S.M., Baxter, B.K., 2020. Great Salt Lake as an astrobiology analogue for ancient martian hypersaline
669 aqueous systems. *Great Salt Lake biology: A terminal Lake in a time of change*, 487–514.

670 Pfeiffer, M., Morgan, A., Heimsath, A., Jordan, T., Howard, A., Amundson, R., 2021. Century scale rainfall in the
671 absolute Atacama Desert: Landscape response and implications for past and future rainfall. *Quaternary*
672 *Science Reviews* 254, 106797.

673 Pruesse, E., Peplies, J., Glöckner, F.O., 2012. SINA: accurate high-throughput multiple sequence alignment of
674 ribosomal RNA genes. *Bioinformatics* 28, 1823–1829.

675 Quade, J., Rech, J.A., Latorre, C., Betancourt, J.L., Gleeson, E., Kalin, M.T.K., 2007. Soils at the hyperarid margin:
676 The isotopic composition of soil carbonate from the Atacama Desert, Northern Chile. *Geochimica et*
677 *Cosmochimica Acta* 71, 3772–3795.

678 Quast, C., Pruesse, E., Yilmaz, P., Gerken, J., Schweer, T., Yarza, P., Peplies, J., Glöckner, F.O., 2012. The SILVA
679 ribosomal RNA gene database project: improved data processing and web-based tools. *Nucleic acids research*
680 41, D590-D596.

681 Rhodes, M.E., Fitz-Gibbon, S.T., Oren, A., House, C.H., 2010. Amino acid signatures of salinity on an
682 environmental scale with a focus on the Dead Sea. *Environmental microbiology* 12, 2613–2623.

683 Robinson, C.K., Wierzchos, J., Black, C., Crits-Christoph, A., Ma, B., Ravel, J., Ascaso, C., Artieda, O., Valea,
684 S., Roldán, M., Gómez-Silva, B., DiRuggiero, J., 2015. Microbial diversity and the presence of algae in halite
685 endolithic communities are correlated to atmospheric moisture in the hyper-arid zone of the Atacama Desert.
686 *Environmental microbiology* 17, 299–315.

687 Sager, C., Airo, A., Arens, F.L., Schulze-Makuch, D., 2021. New type of sand wedge polygons in the salt cemented
688 soils of the hyper-arid Atacama Desert. *Geomorphology* 373, 107481.

689 Sager, C., Airo, A., Arens, F.L., Schulze-Makuch, D., 2022. Eolian erosion of polygons in the Atacama Desert as
690 a proxy for hyper-arid environments on Earth and beyond. *Scientific reports* 12, 12394.

691 Sager, C., Airo, A., Mangelsdorf, K., Arens, F.L., Karger, C., Schulze-Makuch, D., 2023. Habitability of Polygonal
692 Soils in the Hyper-Arid Atacama Desert After a Simulated Rain Experiment. *J. Geophys. Res.*,
693 e2022JG007328.

694 Schulze-Makuch, D., Lipus, D., Arens, F.L., Baqué, M., Bornemann, T.L.V., Vera, J.-P. de, Flury, M., Frösler, J.,
695 Heinz, J., Hwang, Y., Kounaves, S.P., Mangelsdorf, K., Meckenstock, R.U., Pannekens, M., Probst, A.J.,
696 Sáenz, J.S., Schirmack, J., Schloter, M., Schmitt-Kopplin, P., Schneider, B., Uhl, J., Vestergaard, G.,
697 Valenzuela, B., Zamorano, P., Wagner, D., 2021. Microbial Hotspots in Lithic Microhabitats Inferred from
698 DNA Fractionation and Metagenomics in the Atacama Desert. *Microorganisms* 9.

699 Schulze-Makuch, D., Wagner, D., Kounaves, S.P., Mangelsdorf, K., Devine, K.G., Vera, J.-P. de, Schmitt-
700 Kopplin, P., Grossart, H.-P., Parro, V., Kaupenjohann, M., Galy, A., Schneider, B., Airo, A., Frösler, J.,
701 Davila, A.F., Arens, F.L., Cáceres, L., Cornejo, F.S., Carrizo, D., Dartnell, L., DiRuggiero, J., Flury, M.,
702 Ganzert, L., Gessner, M.O., Grathwohl, P., Guan, L., Heinz, J., Hess, M., Keppler, F., Maus, D., McKay, C.P.,
703 Meckenstock, R.U., Montgomery, W., Oberlin, E.A., Probst, A.J., Sáenz, J.S., Sattler, T., Schirmack, J.,
704 Sephton, M.A., Schloter, M., Uhl, J., Valenzuela, B., Vestergaard, G., Wörmer, L., Zamorano, P., 2018.
705 Transitory microbial habitat in the hyperarid Atacama Desert. *Proceedings of the National Academy of
706 Sciences of the United States of America* 115, 2670–2675.

707 Segura, A., Navarro-González, R., 2005. Nitrogen fixation on early Mars by volcanic lightning and other sources.
708 *Geophys. Res. Lett.* 32.

709 Sernageomin, S., others, 2003. Mapa Geológico de Chile: versión digital. Servicio Nacional de Geología,
710 Publicación Geológica Digital 4.

711 Shen, J., 2020. Phospholipid biomarkers in Mars-analogous soils of the Atacama Desert. *International Journal of
712 Astrobiology* 19, 505–514.

713 Stepinski, T.F., Stepinski, A.P., 2005. Morphology of drainage basins as an indicator of climate on early Mars.
714 *Journal of Geophysical Research: Planets* 110.

715 Stern, J.C., Sutter, B., Freissinet, C., Navarro-González, R., McKay, C.P., Archer Jr, P.D., Buch, A., Brunner,
716 A.E., Coll, P., Eigenbrode, J.L., others, 2015. Evidence for indigenous nitrogen in sedimentary and aeolian
717 deposits from the Curiosity rover investigations at Gale crater, Mars. *Proceedings of the National Academy
718 of Sciences* 112, 4245–4250.

719 Stern, J.C., Sutter, B., Jackson, W.A., Navarro-González, R., McKay, C.P., Ming, D.W., Archer, P.D., Mahaffy,
720 P.R., 2017. The nitrate/per chlorate relationship on Mars. *Geophys. Res. Lett.* 44, 2643–2651.

721 Stevenson, A., Cray, J.A., Williams, J.P., Santos, R., Sahay, R., Neuenkirchen, N., McClure, C.D., Grant, I.R.,
722 Houghton, J., Quinn, J.P., others, 2015. Is there a common water-activity limit for the three domains of life?
723 *The ISME journal* 9, 1333–1351.

724 Stoertz and Ericksen, 1974. Geology of the salars of N Chile.

725 Tang, I.N., Munkelwitz, H.R., 1994. Water activities, densities, and refractive indices of aqueous sulfates and
726 sodium nitrate droplets of atmospheric importance. *Journal of Geophysical Research: Atmospheres* 99,
727 18801–18808.

728 Valea, S., 2015. Ecosistemas microbianos endolíticos en nódulos superficiales de halita del desierto hiperárido de
729 Atacama: microclima, microhábitat y biodiversidad.

730 Warren-Rhodes, K.A., Lee, K.C., Archer, S.D.J., Cabrol, N., Ng-Boyle, L., Wettergreen, D., Zacny, K., Pointing,
731 S.B., 2019. Subsurface Microbial Habitats in an Extreme Desert Mars-Analog Environment. *Frontiers in
732 microbiology* 10, 69.

733 Warren-Rhodes, K.A., Rhodes, K.L., Pointing, S.B., Ewing, S.A., Lacap, D.C., Gómez-Silva, B., Amundson, R.,
734 Friedmann, E.I., McKay, C.P., 2006. Hypolithic cyanobacteria, dry limit of photosynthesis, and microbial
735 ecology in the hyperarid Atacama Desert. *Microbial ecology* 52, 389–398.

736 Wickham, H., Chang, W., Wickham, M.H., 2016. Package 'ggplot2'. Create elegant data visualisations using the
737 grammar of graphics. Version 2, 1–189.

738 Wierzchos, J., Ascaso, C., McKay, C.P., 2006. Endolithic cyanobacteria in halite rocks from the hyperarid core of
739 the Atacama Desert. *Astrobiology* 6, 415–422.

740 Wierzchos, J., Cámara, B., Los Ríos, A. de, Davila, A.F., Im Sánchez Almazo, Artieda, O., Wierzchos, K., Gomez-
741 Silva, B., McKay, C., Ascaso, C., 2011. Microbial colonization of Ca-sulfate crusts in the hyperarid core of
742 the Atacama Desert: implications for the search for life on Mars. *Geobiology* 9, 44–60.

743 Wierzchos, J., Los Ríos, A. de, Ascaso, C., 2012. Microorganisms in desert rocks: the edge of life on Earth.
744 *International microbiology : the official journal of the Spanish Society for Microbiology* 15, 173–183.

745 Yang, L., Zhang, Z., Chen, Z., 2021. Formation of nitrite and ammonium during the irradiation of nitrate-
746 containing water by VUV/UV. *Journal of Water Process Engineering* 40, 101801.
747 Zink, K.-G., Mangelsdorf, K., 2004. Efficient and rapid method for extraction of intact phospholipids from
748 sediments combined with molecular structure elucidation using LC-ESI-MS-MS analysis. *Analytical and*
749 *bioanalytical chemistry* 380, 798–812.
750 Ziolkowski, L.A., Wierzechos, J., Davila, A.F., Slater, G.F., 2013. Radiocarbon evidence of active endolithic
751 microbial communities in the hyperarid core of the Atacama Desert. *Astrobiology* 13, 607–616.
752 Zomer, R.J., Xu, J., Trabucco, A., 2022. Version 3 of the Global Aridity Index and Potential Evapotranspiration
753 Database. *Scientific Data* 9, 409.

754 **Acknowledgements**

755 We thank Yunha Hwang for supporting us during the fieldwork. We would like to thank the following people for
756 their contributions to this work: Manuela Alt and Kirsten Weiß from the HU Berlin for conducting the elemental
757 analysis; Ferry Schipperski and Thomas Neumann for the access to their laboratories at the Institut für Angewandte
758 Geowissenschaften at the TU Berlin; Maria Scharfe and Eckhard Flöter from the Institut für
759 Lebensmitteltechnologie und Lebensmittelchemie at the TU Berlin for using their laboratory equipment. Landsat-
760 8 image courtesy of the U.S. Geological Survey. We acknowledge support by the European Research Council
761 Advanced Grant Habitability of Martian Environments (#339231).

762 **Competing interests**

763 The authors declare no competing interests.

764 **Data availability**

765 The authors declare that all the data supporting the findings of this study are available within the article and its
766 Supplementary Information file, or available from the corresponding author on request. Sequence data that support
767 the findings of this study will be deposited in the European Nucleotide Archive with the primary accession code
768 PRJEB70476.

769 **Author contributions**

770 F.A.: conceptualization, fieldwork, sample preparation, XRD measurement, water analysis, ATP analysis, data
771 evaluation and visualization, manuscript writing; A.A.: conceptualization, fieldwork, data evaluation, manuscript
772 writing; C.S.: fieldwork, PLFA measurements, manuscript writing; H.P.G.: genomic data evaluation; K.M.:
773 PLFA data evaluation; R.M.: ATP data evaluation; M.P.: ATP measurement and data evaluation; P.S.K.: organic
774 matter data evaluation; J.U.: organic matter measurement and data evaluation; B.V.: conducting cultivation
775 experiment and genomic analysis; P.Z.: cultivation experiment data evaluation; L.Z.: genomic analysis and data
776 analysis; D.S.M.: project supervision; all authors modified and revised the manuscript.